Discrete models for the formation and evolution of spatial structure in dissipative systems

Gian-Luca Oppo and Raymond Kapral
Chemical Physics Theory Group, Department of Chemistry, University of Toronto, Toronto, Ontario, Canada M5S 1A1
(Received 30 December 1985)

The dynamical structure of systems of coupled discrete-space, discrete-time oscillators is described. The behavior of these systems is considered for different forms of the coupling term, and parallels with cellular automaton models are pointed out. An analysis of the dynamics of dislocation structures is made and the mechanisms for their creation and destruction are discussed. Chaotic spatial patterns may arise near intermittency transitions and the mechanisms which give rise to these structures are studied. External noise can have important effects on the character of spatial patterns and their evolution; such effects are also briefly considered.

I. INTRODUCTION

The formation of spatial structures is a feature common to many physical processes. In the far-from-equilibrium regime the nature of such structures and their evolution takes on special importance. Strong turbulence in fluid flow is one familiar case; morphogenetic processes in living systems is another. Some of the best-characterized spatial structures are found in chemical systems. The Belousov-Zhabotinskii reaction is a chemical example of an excitable medium, which displays expanding rings, target patterns, spiral waves, etc.[1] All of the above processes can be modeled by nonlinear partial differential equations whose behavior is difficult to determine and organize.

As a result of the complexity of such processes and the difficulties associated with the analysis of their differential equation models it is useful to attempt to construct simpler models which are more tractable, both mathematically and computationally, yet are able to capture the essential physics of the process. Perhaps the most familiar of such simpler models of spatial and temporal structure development are cellular automata.[2] In these highly idealized models both space and time are discrete; the allowed values of a dynamical variable are also discrete.

In spite of the simplification of the physical process imposed by these restrictions, automaton models are capable of describing many features of physical processes. The excitable-medium automaton[3] provides an example: a simple three-state, two-dimensional automaton displays the rings, target patterns, and spiral waves mentioned above and gives some insight into the nature of the initial states that produce them. Also the automaton can serve as a guide to the more complex patterns that arise in three dimensions.[4]

In this paper we study a related but different class of models for such processes: coupled-map models.[5–8] For these models space and time are again discrete but the dynamical variables are allowed to take on a continuum of values determined by a multidimensional nonlinear map. Parameters describing the nature of the nonlinear (isolated) oscillators and their coupling can be varied to alter the space-time dynamical behavior of the system. The fact that control-parameter variations are used to change the dynamical state of the system, as in physical processes, along with the fact that conventional bifurcation analyses are easily carried out, make these models attractive for the analytic study of spatio-temporal structure.

A number of general features of such systems are studied here. We focus primarily on cases where the dynamical variables at a site, in isolation of its neighbors, oscillate in time. We then investigate the nature of the spatial and temporal structure that develops when the oscillators are coupled. Many chemical and biological systems have the feature that they oscillate in their bulk "well-stirred" state and develop patterns in space in the absence of stirring or strong diffusion.[1,9] The models we study here may be taken as crude descriptions of some of the phenomena that are seen in systems like these.[10]

After a description of some of the general features of these models in Sec. II, we turn to a study of spatial structure in Sec. III. In the period-2 regime the isolated oscillators alternate between two states. When coupling is present islands of both phases may coexist separated by dislocation boundaries. Various stability properties associated with the coexistence and morphology of the two phases are discussed. Section IV is devoted to a study of the different types of intermittency that are observed for parameter values close to that where period 3 arises in the isolated oscillator by a tangent mechanism. Within the homogeneous period-3 regime various types of behavior are found depending on the nature of the initial condition. In particular some initial states can lead to spatial and temporal chaotic patterns. We describe the mechanism for transitions to such states. In many respects the coupled system behaves like a noisy map and we explore this analogy. In Sec. V we briefly consider some of the phenomena that are observed when an external noise source is added to the coupled-map system. This allows an assessment of the robustness of some of the spatial structures to be made. The results are discussed in Sec. VI.

II. COUPLED-MAP MODELS

Coupled-map models constitute a class of dynamical systems whose space-time evolution is governed by equations of the general form

$$x(\mathbf{i},t+1)=f(x(\mathbf{i},t);\lambda)+c(\mathbf{i},\mathbf{x}(t);\gamma), \tag{2.1}$$

where f is a (nonlinear) function that depends on a set of bifurcation parameters $\lambda=\{\lambda_1,\lambda_2,\ldots\}$, and c is a coupling function, characterized by the parameters $\gamma=\{\gamma_1,\gamma_2,\ldots\}$, that specifies how the discrete-time oscillators interact with each other. Each dynamical variable x is labeled by its site index $\mathbf{i}=\{i_1,i_2,\ldots\}$ in the d-dimensional array, and the discrete time t. The notation $\mathbf{x}(t)$ refers to the set of all $x(\mathbf{i},t)$. We restrict ourselves to the case of periodic boundary conditions so that in one dimension (1D) we have a ring of maps and in 2D the array of maps resides on a torus. A site $\mathbf{i}$ may communicate with surrounding sites in a variety of ways. The coupling may be linear or nonlinear; models of spatially extended physical systems exist where the coupling is of either type. Perhaps the most familiar type of coupling arises from diffusion whose discrete form is

$$\begin{aligned} c(\mathbf{i},\mathbf{x}(t);\gamma)=\gamma\{&[x(i_1+1,i_2,t)+x(i_1-1,i_2,t)\\ &+x(i_1,i_2+1,t)+x(i_1,i_2-1,t)]\\ &-4x(i_1,i_2,t)\}, \end{aligned} \tag{2.2}$$

in 2D with obvious generalization to other dimensions. Such coupling is common in chemical, biological, and hydrodynamic systems, but these systems also provide examples of nonlinear coupling. From Eq. (2.2) it is clear that the discrete form of diffusive coupling leads to interactions among blocks of five neighboring sites on the lattice.

The coupling term can be generalized in a straightforward manner to take into account interactions among $q+1$ sites on the lattice. Let c be proportional to the difference between the value of the dynamical variable at site $\mathbf{i}$ at time t and its sum over q surrounding sites at the same time,

$$c(\mathbf{i},\mathbf{x}(t))=\gamma[X(\mathbf{i},t)-qx(\mathbf{i},t)],$$

with

$$X(\mathbf{i},t)=\sum_j{}'x(\mathbf{j},t), \tag{2.3}$$

where the prime denotes the sum over the q neighbors of site $\mathbf{i}$. Other choices for $X(\mathbf{i},t)$ are possible; for example, we may select a weighted sum over the neighbors of site i.

Since the value of $x(\mathbf{i},t+1)$ depends on $x(\mathbf{i},t)$ and the sum of the values of $x(\mathbf{j},t)$ of its neighbors, this class of models is analogous to cellular automata with outer totalistic rules.[2] The model specifies a continuous transformation from old to new site values, which depends on bifurcation parameters. These parameter variations lead to new dynamical behavior as bifurcation points are crossed, similar to that obtained by rule changes in cellular automata. In most physical systems, changes in behavior are affected by such parameter variation. We also note that like systems with diffusive coupling, the models studied here have the characteristic feature that the coupling term vanishes for the spatially homogeneous state.

Wolfram has organized cellular automata into four classes according to their behavior.[2] Class-1 cellular automata evolve to homogeneous states. In certain regions of the parameter plane the coupled-map model behaves like a class-1 automaton. In such regions the spatially homogeneous state, where all oscillators have the same phase, is stable to small perturbations. It has been shown earlier[5] that the sizes of these regions in the two-parameter plane satisfy universal scaling rules where the scaling parameters are the same as those for the isolated map dynamics.

The spatially homogeneous states play an important part in the understanding of the behavior of these systems since one is often interested in the mechanism by which a uniform system breaks its symmetry to form a spatial structure as a bifurcation parameter is varied. For example, crossing of certain boundaries produces period-doubled inhomogeneous states with wave vector $\mathbf{k}$, i.e., temporally *and* spatially periodic states. These states have many features in common with class-2 cellular automata, which evolve to periodic structures. In other regions of parameter space, especially near intermittency transitions to chaos, the coupled-map model behaves like a class-3 cellular automaton, i.e., it develops chaotic spatial structure. Pattern formation is possible even within the homogeneous regions provided the initial state is removed far enough from the homogeneous state. Thus, depending on the initial state, spatially homogeneous, periodic, or chaotic structure is possible for the same system parameters. This makes the classification of behavior difficult.

In Sec. II A we shall study some of the types of structure which form in different regions of parameter space for different models of the coupling term. All the explicit calculations presented in this paper are carried out for coupled logistic maps where $f(x,\lambda)=\lambda x(1-x)$. Many of the results are independent of the specific form of the nonlinear function but in some circumstances new phenomena are observed for other map functions. Interesting effects are seen when the map has more than one extremum, but this will not be described in this paper.

A. Interaction-model dependence

The homogeneous regions described above have borders which depend on the model for the interactions among sites and on the wave vectors of particular Fourier modes of the array. Crossing of a boundary signals the instability of a particular wavelength mode, but the location of an instability in the (λ,γ) plane depends on the nature of the coupling term. In order to make this point explicit we outline the results for the boundaries of the homogeneous regions given earlier,[5] but now in a form which is valid for the entire class of models considered here, and for any wave vector.

In Fourier space the evolution equation takes the form

$$\xi(\mathbf{k},t)=\hat{f}(\xi(t);\lambda)+\hat{c}(\mathbf{k},\xi(t)),$$

with

$$\hat{c}(\mathbf{k},\xi(t))=u(\mathbf{k})\xi(\mathbf{k},t), \tag{2.4}$$

where $\xi(\mathbf{k},t)$ denotes the Fourier transform of $x(\mathbf{i},t)$,

$$\xi(\mathbf{k},t)=N^{-d}\sum_j \exp(-2\pi i\,\mathbf{j}\cdot\mathbf{k}/N)x(\mathbf{j},t)\ . \tag{2.5}$$

In Eq. (2.4), $\hat{f}(\xi(t);\lambda)$ and $\hat{c}(\mathbf{k},\xi(t))$ are the transforms of f and c. The linear stability analysis of the periodic

homogeneous states leads to the bifurcation condition

$$\prod_{\alpha=1}^{n} [f'(x_\alpha^*;\lambda)+u(\mathbf{k})]=\pm 1 \ . \tag{2.6}$$

This equation yields boundary curves in the (λ,u) plane which determine the stability regions corresponding to spatially homogeneous period-n states. The boundary curves of these regions depend on the coupling only through $u(\mathbf{k})$. Thus, the results for all models in this class for all $\mathbf{k}$ values (for a particular f) may be obtained simply by scaling the u axis. Analysis of Eq. (2.6) for the period-doubled states leads directly to the scaling relation discussed earlier.[5] As an example, the "universal" boundary curves for the period-3 states are shown in Fig. 1. We shall discuss some special features of these curves in Sec. IV. For an $N\times N$ square array of maps there are $M=N(N/2-1)/2$ wave vectors to consider. Thus for a particular model each boundary curve in the (λ,u) plane is split into M curves, which may be simply obtained from the original curve. The boundary curves are parabolic in shape near their minima, and the minima for all the curves derived by scaling u lie along lines with λ constant.

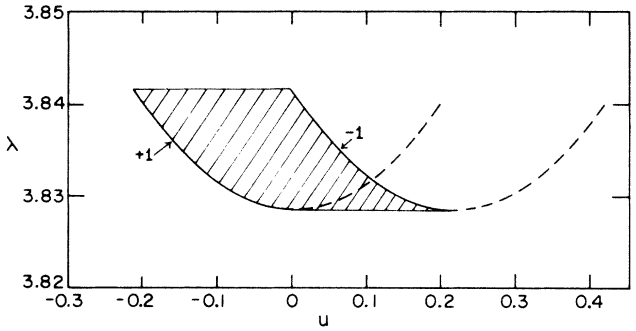

FIG. 1. "Universal" boundaries in the (λ,u) plane corresponding to period-3 spatially homogeneous states. Results for different models are obtained by scaling the u axis.

We noted above that crossing of a boundary signals the appearance of a spatially inhomogeneous state. In particular, when a boundary corresponding to -1 in Eq. (2.6) is crossed, an inhomogeneous period-doubled state appears.

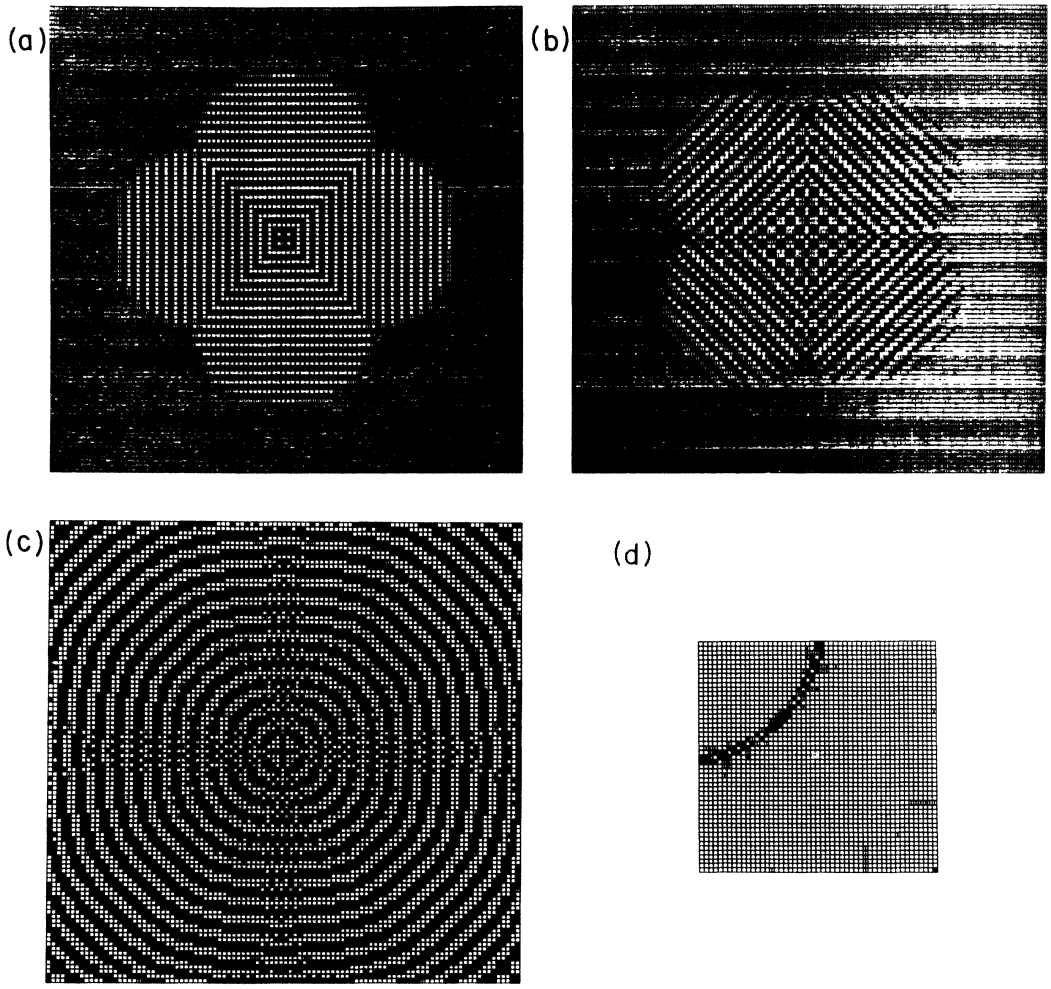

FIG. 2. Evolution from an initial seed for a 100×100 two-dimensional array of maps: (a) nine-neighborhood model with ($\lambda=3.30$, $8\gamma=-0.4$) at $t=400$, (b) thirteen-neighborhood model with ($\gamma=3.30$, $12\gamma=-0.4$) at $t=400$, (c) thirteen-neighborhood model with ($\lambda=3.30$, $12\gamma=-1.0$) at $t=400$. The shading of a square indicates the magnitude of x at that site. (d) Spatial Fourier transform of the pattern given in (c).

The change in the interaction model reorganizes the boundary curves in the (λ,γ) plane so that rather different spatial structures are observed at corresponding parameter values. Consider the five-, nine-, and thirteen-neighborhood models as examples. For diffusive coupling in a 2D array (five-neighborhood model) $u(\mathbf{k})$ takes the form

$$u(\mathbf{k})=4\gamma\{\cos[\pi(k_1+k_2)/N]\cos[\pi(k_1-k_2)/N]-1\}, \tag{2.7}$$

while for the nine-neighborhood model $u(\mathbf{k})$ is

$$u(\mathbf{k})=2\gamma\{\cos[2\pi(k_1+k_2)/N]+\cos[2\pi(k_1-k_2)/N] +2\cos[\pi(k_1+k_2)/N] \times\cos[\pi(k_1-k_2)/N]-4\}, \tag{2.8}$$

and for the thirteen-neighborhood model we have

$$u(\mathbf{k})=2\gamma\{\cos[2\pi(k_1+k_2)/N]+\cos[2\pi(k_1-k_2)/N] +2\cos[2\pi(k_1+k_2)/N]\cos[2\pi(k_1-k_2)/N] +2\cos[\pi(k_1+k_2)/N] \times\cos[\pi(k_1-k_2)/N]-6\}. \tag{2.9}$$

Using the above values of $u(\mathbf{k})$ one may determine the nature of the instabilities for the different models. The first instability crossed in moving away from $\gamma=0$ is that with wavelength 2 in both lattice directions for the five-neighborhood model, which leads to a checkerboard pattern; this type of instability determines the behavior in a relatively large region in parameter space. If instead one considers the nine-neighborhood model the main instability type is one with wavelength equal to 2 in one lattice direction and infinite wavelength in the other. Of course, this state is double degenerate. The dominant type of pattern is one of horizontal or vertical stripes. Evolution from initial seeds produces expanding rings for small times, which later fragment [see Fig. 2(a)], rather than a checkerboard pattern as in the five-neighborhood model. The results for the thirteen-neighborhood model are shown in Fig. 2(b). Here the dominant instability corresponds to a wavelength of 4 in each direction.

Beyond the region corresponding to these major instabilities there is a complex region of boundary crossings where each pure mode occupies a very small region of the parameter plane; here the inhomogeneous structure is determined by mixtures of the pure mode states. The character of the structure in these regions is also model

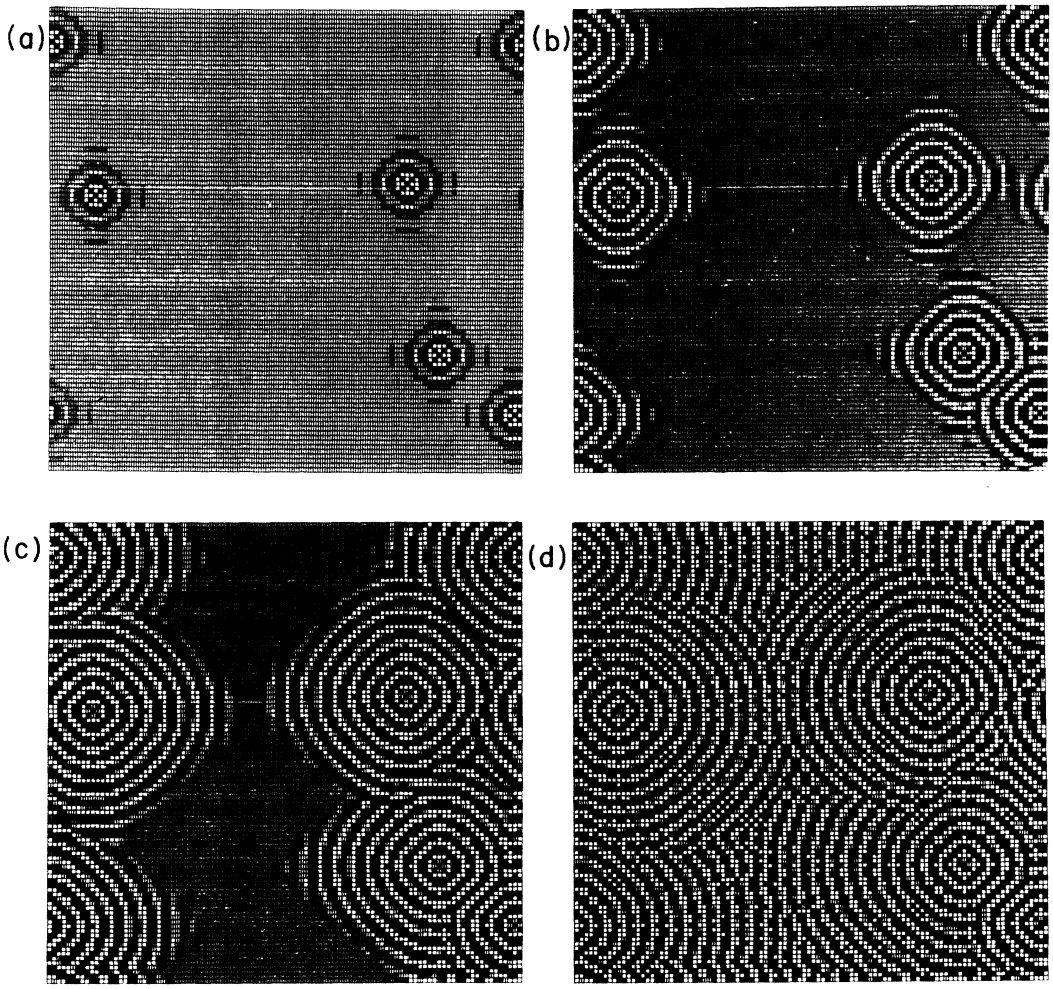

FIG. 3. Evolution from a random spatial distribution of five initial seeds for the two-dimensional nine-neighborhood model with ($\lambda=3.30$, $\gamma=-0.125$) at (a) $t=40$, (b) $t=80$, (c) $t=120$, and (d) $t=1600$.

dependent since the nature of the mixture of states varies from model to model. Two examples will illustrate the types of pattern possible. In Fig. 3 a series of pictures shows how a random distribution of five initial seeds evolves as a function of time for parameter values ($\lambda=3.30$, $\gamma=-0.125$) for the nine-neighborhood model. A set of concentric rings develops from each initial inhomogeneity. The pattern does not consist of traveling waves, rather the outermost ring of excitation induces the formation of the next ring, while maintaining its integrity. At later times the rings from different regions collide and annihilate forming a structure that resembles the target patterns of the Belousov-Zhabotinskii reaction, but the mechanism giving rise to the structure is quite different. However, it is possible to construct coupled-map models which can simulate the behavior of an excitable medium like the Belousov-Zhabotinskii reaction.

As another example Fig. 2(c) shows the growth of a pattern from a single seed for the thirteen-neighborhood model in a region of parameter space where even more complicated spatial periodic behavior is observed. The spatial periodic character of this structure is revealed by examining the pattern in Fourier space. Panel (d) in Fig. 2 shows the magnitude of the complex Fourier transform of the real-space pattern. The wave vectors lie on an arc in the $\mathbf{k}$ plane with center at $\mathbf{k}=(0,0)$.

III. DISLOCATION STRUCTURES

Many different spatially inhomogeneous states are possible in coupled-map systems. Their nature depends not only on the map model and its parameters but also on the initial state, since multistability among the various attracting states is possible. Even in the spatially homogeneous regions different initial states can lead to complex structures with dislocations due competition among states with similar stability. This is possible since the linear stability analysis which was used to derive the boundaries of the homogeneous regions only guarantees that such states are stable to small perturbations. It does not rule out the possibility of multistability; other coexisting states may be accessible from different initial conditions.

Consider a simple illustration of this phenomenon. In the spatially homogeneous period-2 region the fixed-point structure is identical to that for an isolated map with period 2. If an array or a ring of such maps is considered, with no coupling among the oscillators, then each oscillator may exist in either of the phases of the period-2 cycle. One might then inquire about the nature of the final state when the oscillators are coupled, given that there is an initial random spatial distribution of the two phases, an initial state far removed from the homogeneous state where all oscillators are in phase. This type of initial condition takes on added importance since relaxation to the stable period-2 cycle is rapid. Hence, an arbitrary initial state will, after a few time steps, relax close to the random-phase initial condition. Subsequent relaxation to the final attracting state will take place on a much longer time scale. As time progresses homogeneous patches of either phase develop, which are separated by dislocation ("kink" and "antikink") boundaries. The long-time evolution of the system depends on the interactions and motions of these dislocation boundaries.[11] The sharpness of the boundaries depends on the interaction strength; the stronger the interaction the more diffuse the boundary. For large interaction strengths, small nearly homogeneous regions will not persist and the spatial structure will consist of large patches of regions of equal phase. Spatial structure of this type is shown in Figs. 4(a) and 4(b) for the two-dimensional case. When the interaction strength is small the dislocation boundaries are sharp and small homogeneous regions may remain stable [see Fig. 4(c)].

The above observations apply to the zones corresponding to higher periods as well. In this case the spatial structure is more complicated due to the fact that the number of possible initial phases is greater. An example of the spatial structure for the period-4 case is shown in Fig. 4(d).

Similar dislocation structures are observed in arrays of maps with d dimensions. The one-dimensional case is especially simple since the final state consists of blocks of cells with nearly the same phase.[6] An example of the type of structure observed can be seen in Fig. 5(a) where the time evolution of an initial random-phase state is shown. One can see in the time history the competition among the different size blocks. In order to investigate this case in more detail, consider an initial state where almost all the oscillators in the ring are initially in phase except for a small number (n) of contiguous oscillators, which are set out of phase. Solutions of this type are stable provided the coupling strength is smaller than a threshold value $\gamma_c(n)$, which depends on n. The numerically measured thresholds for different values of n are reported in Table I. Insight into the mechanism of the instability can be obtained from Fig. 5(b), which shows the first and the second iterates of the single "out-of-phase" map for $n=1$ for γ slightly larger than the threshold $\gamma_c(1)$. The average effect of the rest of the oscillators in the ring is to give a two-dimensional character to the out-of-phase map so that its second iterate appears to be composed of two branches. This behavior is reminiscent of the dynamics observed in a map with additive dichotomous noise,[12] and some parallels between coupled maps and noisy maps can

TABLE I. Critical values of the coupling γ_c as a function of the length n of the block of out-of-phase oscillators for $\lambda=3.2$.

n	$\gamma_c(n)$
1	−0.027 715
2	−0.060 570
3	−0.095 784
4	−0.131 174
5	−0.165 958
6	−0.200 117
7	−0.233 910
8	−0.267 523
9	−0.301 194
10	−0.335 178
11	−0.369 752
12	−0.405 356
13	−0.442 821

be made. However, the process described here is completely deterministic and successive iterates of the map alternate between the two curves. Increasing γ leads to a progressive splitting of the two branches until a situation akin to a tangent bifurcation is reached; the out-of-phase map loses its stability and relaxation to the in-phase state occurs.

The validity of this picture can be checked by introducing an average coupling term Δ in the equation for the out-of-phase map, which we take to be located at position i,

$$x(i,t+1)=g(x(i,t),\Delta) =\lambda x(i,t)[1-x(i,t)]+\Delta\ . \tag{3.1}$$

The λ dependence of g has been suppressed for notational convenience. We note that the sign of Δ changes at every iterate. At the tangent threshold we impose the conditions

$$x^*(i)=g^{(2)}(x^*(i),\Delta_c)\,, \tag{3.2a}$$

$$\frac{\partial g^{(2)}(x^*(i),\Delta_c)}{\partial x(i)}=1\,, \tag{3.2b}$$

from which both the fixed point $x^*(i)$ and the critical value Δ_c can be calculated.

Since Δ_c is small, we can reduce the order of Eq. (3.2a) by using an expansion valid to first order in Δ_c. Imposing the tangent condition, we have

$$\Delta_c=\frac{\lambda(1+\lambda)}{4}\frac{(3x_1^2-4x_1+4/\lambda)(3x_1^2-4x_1+1+1/\lambda)}{x_1^2(3+2\lambda)-2x_1(2+\lambda)+2+2/\lambda}\,,$$
$$x^*(i)=1-\frac{x_1}{2}+\frac{\Delta_c}{\lambda(1+\lambda)}\frac{\lambda x_1^2-x_1(1+2\lambda)+1+\lambda}{3x_1^2-4x_1+1+1/\lambda}\,, \tag{3.3}$$

where

$$x_1=(2\lambda)^{-1}[\lambda+1\pm\sqrt{(\lambda+1)(\lambda-3)}]\,, \tag{3.4}$$

are the period-2 fixed points of the uncoupled map. In Table II the analytical results are compared with the numerical solution of Eq. (3.2) and with the computed

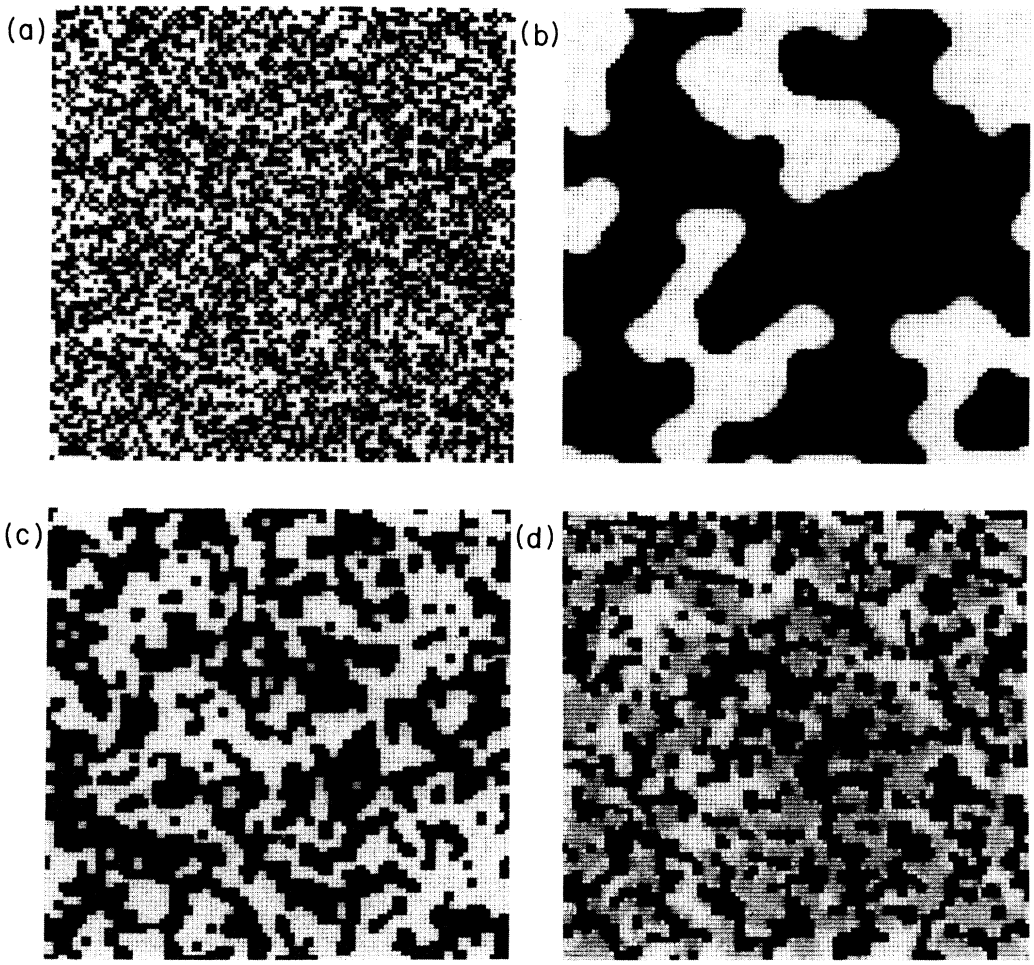

FIG. 4. Time evolution from an initial random-phase distribution for the two-dimensional five-neighborhood model with (a) ($\lambda=3.2$, $\gamma=-0.05$), period-2 region, at $t=2$, (b) ($\lambda=3.2$, $\gamma=-0.05$), period-2 region at $t=4000$, (c) ($\lambda=3.2$, $\gamma=-0.025$), period-2 region, at $t=4000$, and (d) ($\lambda=3.48$, $\gamma=-0.035$), period-4 region, at $t=4000$.

TABLE II. Comparison of the numerical simulations of the coupled-map model, the solutions of Eqs. (3.2) and (3.5) using Newton's method, and the analytical result, Eq. (3.3), for the critical coupling term Δ_c and the fixed points x_1^* and x_2^* for $\lambda=3.2$ and $n=1$.

	Numerical Simulation	Eq. (3.2)	Eq. (3.3)	Eq. (3.5)
Δ_c	−0.012 118	−0.011 198	−0.010 296	−0.012 070
	−0.010 172			−0.010 083
x_1^*	0.753 065	0.760 749	0.759 987	0.752 022
x_2^*	0.607 184	0.593 631	0.592 601	0.608 822

values. Note that using the value of $\gamma_c(1)$ and the fixed points obtained by direct iteration, two values of Δ_c are available, one corresponding to each period-2 phase. Since we have considered the average effect of all in-phase oscillators on the one which is out of phase, this asymmetry does not appear in the one-map theory.

Although the agreement between this simple theory and the direct computations is quite good, it is possible to generalize the method by considering the following set of equations:

$$\begin{aligned} x(i,t+1)&=\lambda x(i,t)[1-x(i,t)]+2\gamma[x(i+1,t)-x(i,t)] \\ x(i+1,t+1)&=\lambda x(i+1,t)[1-x(i+1,t)] \\ &\quad+\gamma[x(i,t)+x_1-2x(i+1,t)], \end{aligned} \tag{3.5}$$

where x_1 is given by Eq. (3.4), with the suitable fixed point chosen for each iterate. All oscillators except the ith and its nearest neighbors are assumed to have the same value x_1. Thus, the explicit effect of the nearest-neighbor oscillators is included. As in the earlier calculation, the tangent condition is applied to the ith oscillator. The numerical solution of Eq. (3.5), using Newton's method, is shown in the last column of Table II and provides a test of the theory. In addition, the case $n=2$ is immediately recovered if 2γ is replaced by γ in the first of Eqs. (3.5).

For larger values of n, the tangent mechanism continues to operate but more complicated coupling effects make a simple description like that of Eq. (3.5) difficult to formulate. However, if we suppose all the out-of-phase oscillators may be treated as an average oscillator with value x', and write an equation for this average value, we obtain

$$\begin{aligned} x'(i,t+1)&=\lambda x'(i,t)[1-x'(i,t)] \\ &\quad+(2\gamma/n)[x(i+1,t)-x'(i,t)], \end{aligned} \tag{3.6}$$

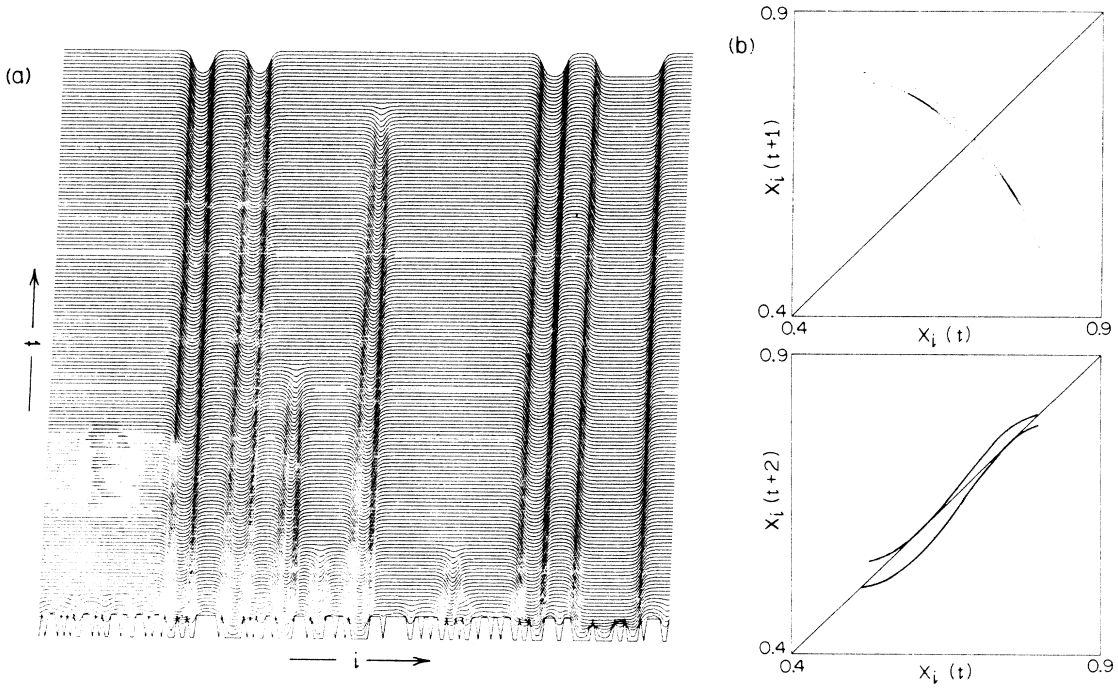

FIG. 5. (a) Time evolution of an initial random distribution of the two period-2 phases for 200 coupled maps in a one-dimensional chain. The ordinate is time and the abscissa is the site index. The results are plotted every two time steps up to $t=320$ with ($\lambda=3.2$, $\gamma=-0.25$). (b) First and second next-amplitude maps for the single out-of-phase oscillator in an otherwise homogeneous chain with ($\lambda=3.2$, $\gamma=-0.02775$). Solid lines have been drawn through the points in order to make the "tangent character" of the map evident.

where $x'(i,t)$ is the effective dynamical variable for the entire block of length n. Replacing the first equation of (3.5) by (3.6), a rough estimate of the thresholds for $n>2$ can be made. In spite of the crude nature of these assumptions, the final error is, for example, less than 20% for $n=7$. The explicit form of the coupling term in Eq. (3.6) also explains the linear variation of $\gamma_c(n)$ with n, which is observed in the numerical simulations (Table I).

We can now ask how the existence of the thresholds $\gamma_c(n)$ affects the dynamics of the one-dimensional model. We once again use initial states with randomly distributed phases. For fixed values of the coupling parameter γ, we evaluated the number of patches with a certain length after transients were discarded. The results for four values of γ are reported in Fig. 6. As the coupling is increased small patches are no longer stable and the initial exponential distribution [see Fig. 6(a)] is destroyed since patches of large size are favored [Figs. 6(b)—6(d)]. Percolation and phase-transition thresholds can be defined in both the two- and three-dimensional models.

Dislocation structures are also observed in regions of the parameter plane where strictly alternating states are stable. These alternating states arise by a subharmonic bifurcation process where the in-phase (infinite wavelength) states lose stability and an out-of-phase state with a wavelength of 2 is born.[5] One may now have patches of oscillators with different registrations of the alternating pattern (Fig. 7).

In contrast to the homogeneous states, the alternating states may lose their stability through a Hopf bifurcation, which gives rise to invariant circles in the vicinity of each out-of-phase fixed point. The existence of these invariant circles can have an important effect on the dynamics of the dislocation boundaries separating the alternating states with different registration. Indeed, for parameter values close to and larger than those corresponding to the Hopf boundary, the kink and antikink boudnaries can propagate along the chain and annihilate upon collision. This process leads to an increase in the average length of the patches of alternating sites; far enough from the Hopf boundary the strictly alternating state on the chain is reached (Fig. 7).

This effect is similar to that of added noise, which is discussed in Sec. V and implies that the stability of states with dislocations is connected to the fixed point nature of the maps. Any stochastic (external noise) or deterministic (like the Hopf bifurcation described above) perturbation of the fixed point leads to the progressive destruction of these spatial irregularities and enlarges the region of parameter space where the perfect "crystalline" state is observed.

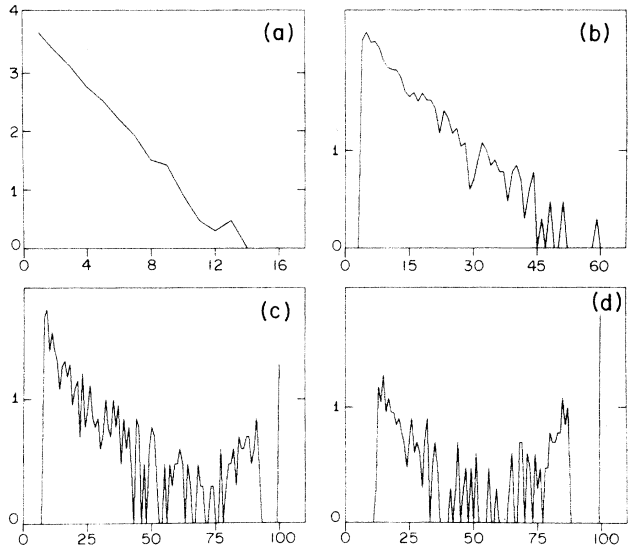

FIG. 6. Plot of the $\log_{10}$ of the average number of blocks of in-phase oscillators of length n vs n for a chain of 100 coupled maps with $\lambda=3.2$. The average was computed over 200 realizations of the random-phase initial conditions. (a) $\gamma=-0.02$, (b) $\gamma=-0.11$, (c) $\gamma=-0.25$, and (d) $\gamma=-0.39$. For (b), (c), and (d), γ is sufficiently large that small blocks are not allowed, hence, the gap in the plot.

IV. SPATIAL STRUCTURES NEAR INTERMITTENCY TRANSITIONS

The spatial structure that appears close to the intermittency threshold is discussed in this section. Some related qualitative results for the behavior in this region have been presented by Kaneko.[8]

We shall focus on the dynamics of the coupled-map model in and near the homogeneous period-3 region in the two-parameter plane. This is one of the most prominent regions where intermittency is observed for the logistic map. The boundaries of these in-phase regions were shown in Fig. 1. They have a form different from those of the period-doubling sequence.[5] While each curve corresponding to ±1 in Eq. (2.6) has a locally parabolic shape, one half of the curve (dashed) is obtained from the unstable fixed point of the stable-unstable pair generated at the tangent bifurcation and is, therefore, irrelevant for determining the stability region. The relevant branches of the curves are joined by straight lines at the top and bottom of the region at the bifurcation points of the uncoupled system. These straight lines correspond to the $\mathbf{k}=0$ (infinite wavelength) boundary curves. Thus, the tangent bifurcation point of the logistic map is drawn out into a line $\lambda=1+\sqrt{8}$ in the (λ,γ) plane for the coupled-map model.

Within these boundaries the synchronized state is stable to small perturbations but, as discussed earlier for the period-2 and period-4 regions, large perturbations from this state can lead to other coexisting attractors. Consider the evolution of a single-seed perturbation in an otherwise homogeneous one-dimensional ring. Beyond a critical amplitude ϵ_c of the seed (i.e., the distance from the in-phase point) a dramatic change of the evolution occurs. For amplitudes less than ϵ_c the in-phase period-3 solution is restored after a transient period. On the other hand, for $\epsilon>\epsilon_c$ the chaotic evolution of the perturbed oscillator propagates along the chain inducing spatial disordered patterns like those shown in Fig. 8(a). It is important to note that ϵ_c is always much smaller than the coordinate

shift of the out-of-phase solution. This implies that, for every value of the coupling, random-phase initial conditions evolve towards chaotic states; the probability of reaching the in-phase solution is very small within the entire "homogeneous" region of Fig. 1.

A mean-field-like theory for predicting the critical amplitude ϵ_c can be constructed. Consider a single map in the chain displaced from its in-phase period-3 value by an amount ϵ. Assuming the nearest neighbors of the perturbed map are not affected by its dynamics, the evolution of the initial dephasing ϵ is governed by the following map:

$$\epsilon' = F^{(3)}(\epsilon), \tag{4.1a}$$

where

$$F(\epsilon) = \lambda\epsilon[1-2(y+\gamma/\lambda)-\epsilon], \tag{4.1b}$$

with

$$y' = f(y) = \lambda y(1-y).$$

The above equations apply for λ values inside the in-phase period-3 stability region (Fig. 1), and homogeneous initial conditions y equal to one of the three fixed points of the logistic map for all other oscillators. For the parameter values of interest, the map (4.1) has a nearly parabolic shape and possesses a stable fixed point at $\epsilon=0$ and an unstable one at a positive value of ϵ. The boundaries of the immediate basin of attraction of $\epsilon=0$ provide a good estimate of $\epsilon_c^{\pm}$, where + and − label the sign of the perturbation from the in-phase periodic solution [see Fig. 8(b)]. The basin boundaries are given by the unstable fixed point and its preimage, which can be evaluated using Newton's method. The results are compared with direct measurements in Table III. The best agreement is found for small values of γ where the mean-field approximation is expected to be accurate. It is worthwhile to notice that

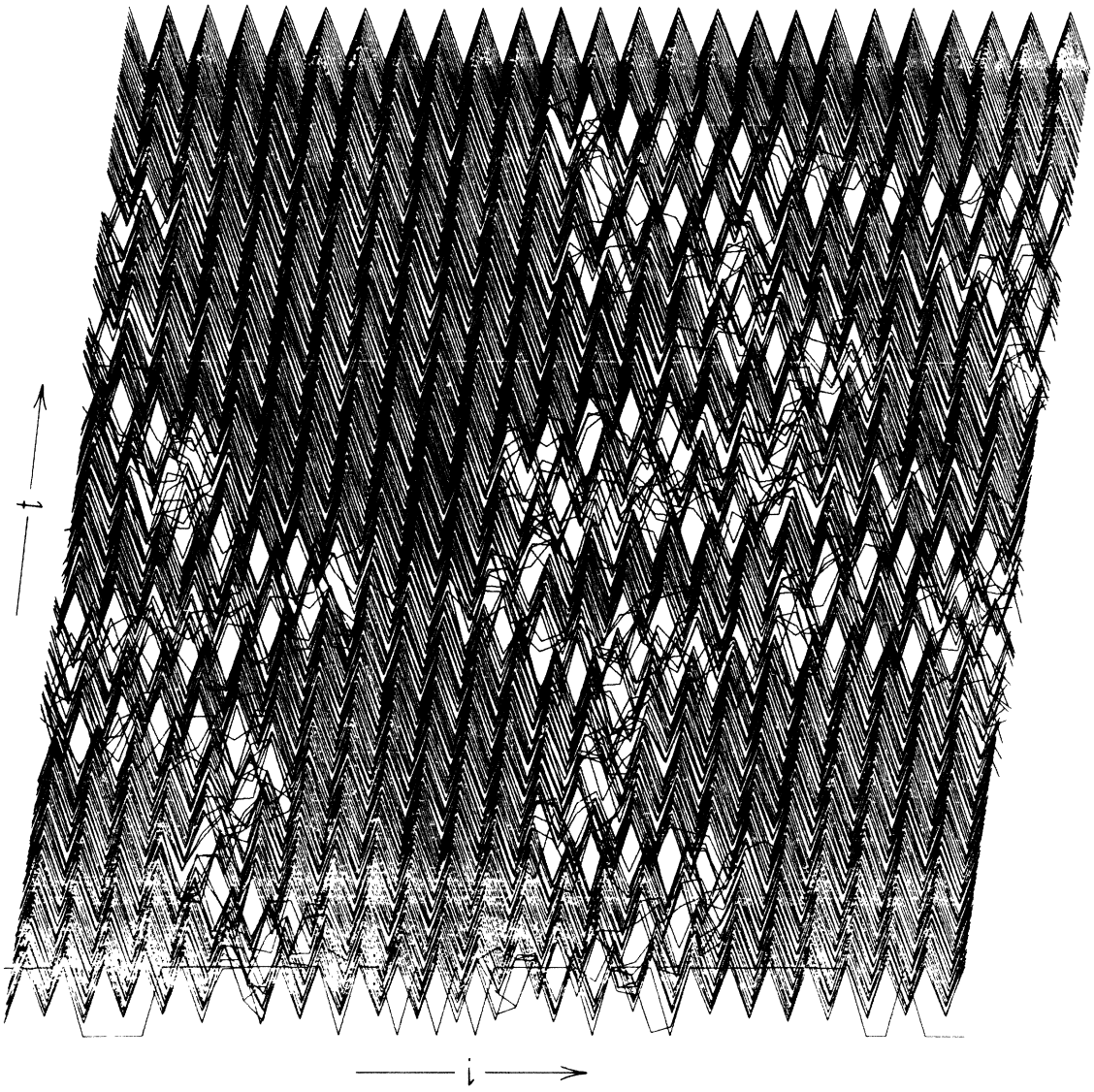

FIG. 7. Dislocation dynamics in a strictly alternating pattern. Starting from a random-phase initial condition with ($\lambda=3.748$, $\gamma=-0.07$), a purely alternating state is reached after approximately 13 000 time steps.

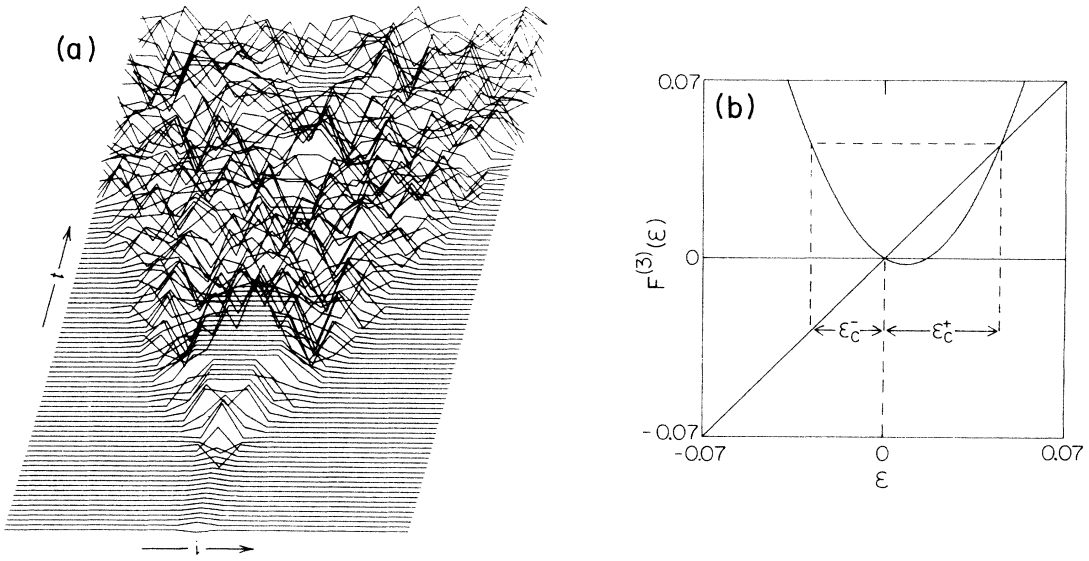

FIG. 8. (a) Time evolution of an initial seed in a homogeneous period-3 chain with ($\lambda=3.835$, $\gamma=-0.01$). The results are plotted every three time steps up to $t=300$. (b) Plot of the map (4.1) for ($\lambda=3.835$, $\gamma=-0.01$), which governs the evolution of the initial dephasing ϵ. The critical dephasing amplitudes $\epsilon_c^{\pm}$ are shown in the diagram.

at the bifurcation point ($\lambda_c=1+\sqrt{8}$) and small values of γ, a finite ϵ_c^- always exists. Indeed, expanding $F^{(3)}(\epsilon)$ close to $\epsilon=0$ we obtain

$$F^{(3)}(\epsilon)=a\epsilon(c-\epsilon), \tag{4.2}$$

where

$$a(\lambda,\gamma)=\lambda^3 Q,$$

and

$$c(\lambda,\gamma)=Q^{-1}\nu_0\nu_1\nu_2,$$

with

$$Q(\lambda,\gamma)=\lambda^2(\nu_0\nu_1)^2+\lambda\nu_0^2\nu_2+\nu_1\nu_2,$$

where we have defined

$$\nu_i=1-2(y_i+\gamma/\lambda),\quad y_i=f^{(i)}(y),\quad i=0,1,2\ .$$

From Eq. (4.2) the unstable fixed point and its preimage can be determined. We find

$$\epsilon_c^+=c-1/a,\quad \epsilon_c^-=1/a\ . \tag{4.3}$$

For small values of $(\lambda-\lambda_c)$ and γ, these critical amplitudes take the forms

$$\epsilon_c^+=(c_\lambda-\alpha_\lambda)(\lambda-\lambda_c)^{1/2}+(c_\gamma-\alpha_\gamma)\gamma, \tag{4.4}$$

and

$$\epsilon_c^-=\alpha_0+\alpha_\lambda(\lambda-\lambda_c)^{1/2}+\alpha_\gamma\gamma,$$

where the $(\lambda-\lambda_c)^{1/2}$ terms arise from the λ dependence of the fixed point y of the unperturbed map. The c_λ, c_γ,

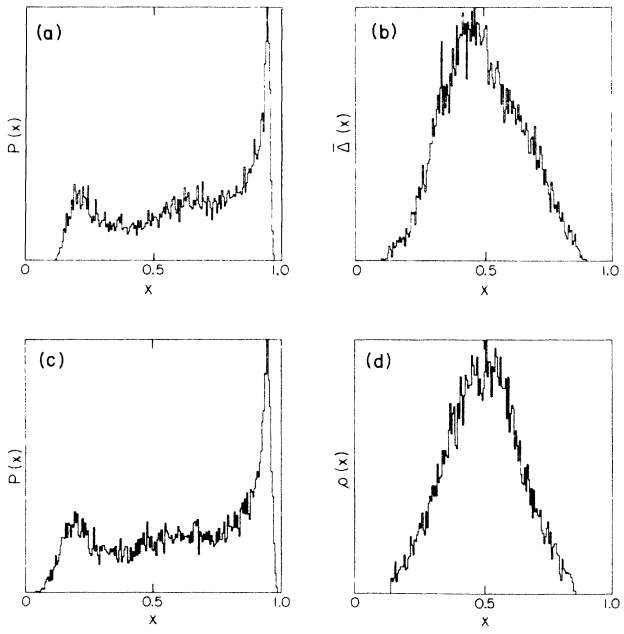

FIG. 9. Comparison between the coupled-map system and a single noisy map. (a) Invariant density $P(x)$ on the unit interval of x for a single map in a coupled-map chain with ($\lambda=3.83$, $\gamma=-0.02$) (random-phase initial condition). (b) Probability distribution of the coupling term $\bar{\Delta}(x)$ normalized to the unit interval, for the conditions in (a). (c) Invariant density $P(x)$ for a single map with added Gaussian noise. (d) The probability distribution of the Gaussian noise. This was roughly scaled to match $\bar{\Delta}(x)$ in (b). The invariant densities in (a) and (c) are quite similar.

TABLE III. comparison between the numerical simulations of the coupled-map model and the solution of Eq. (4.1) using Newton's method, for the critical dephasing $\epsilon_c^{\pm}$ for parameter values within the stability region of the in-phase period-3 solution.

		Numerical simulation		Mean-field model	
λ	γ	ϵ_c^+	ϵ_c^-	ϵ_c^+	ϵ_c^-
3.828 5	−0.002	0.005 16	−0.028 72	0.005 22	−0.028 72
3.828 5	−0.010	0.008 47	−0.028 61	0.009 43	−0.028 76
3.828 5	−0.030	0.013 92	−0.026 99	0.019 98	−0.028 86
3.830 0	−0.002	0.020 37	−0.028 68	0.020 39	−0.028 68
3.830 0	−0.010	0.024 30	−0.028 70	0.024 60	−0.028 71
3.830 0	−0.030	0.032 85	−0.028 32	0.035 14	−0.028 81
3.835 0	−0.002	0.040 55	−0.028 54	0.040 55	−0.028 54
3.835 0	−0.010	0.044 60	−0.028 57	0.044 76	−0.028 57

α_λ, and α_γ coefficients can be expressed in terms of derivatives of the map function (4.1). In the case of $\lambda=\lambda_c$ and $\gamma=0$, ϵ_c^- is found to be equal to $-0.0292\ldots$, in good agreement with the numerical computations. Moreover, expression (4.4), describing the growth of the trapping region, also gives some hint about the probability of observing in-phase solutions starting from random-phase initial conditions, after a chaotic transient period.

The theory presented here can be applied to other forms of $f(y)$ as well and can, for example, provide a description of the mechanism of the self-similar growth of laminar regions in coupled circle maps.[8]

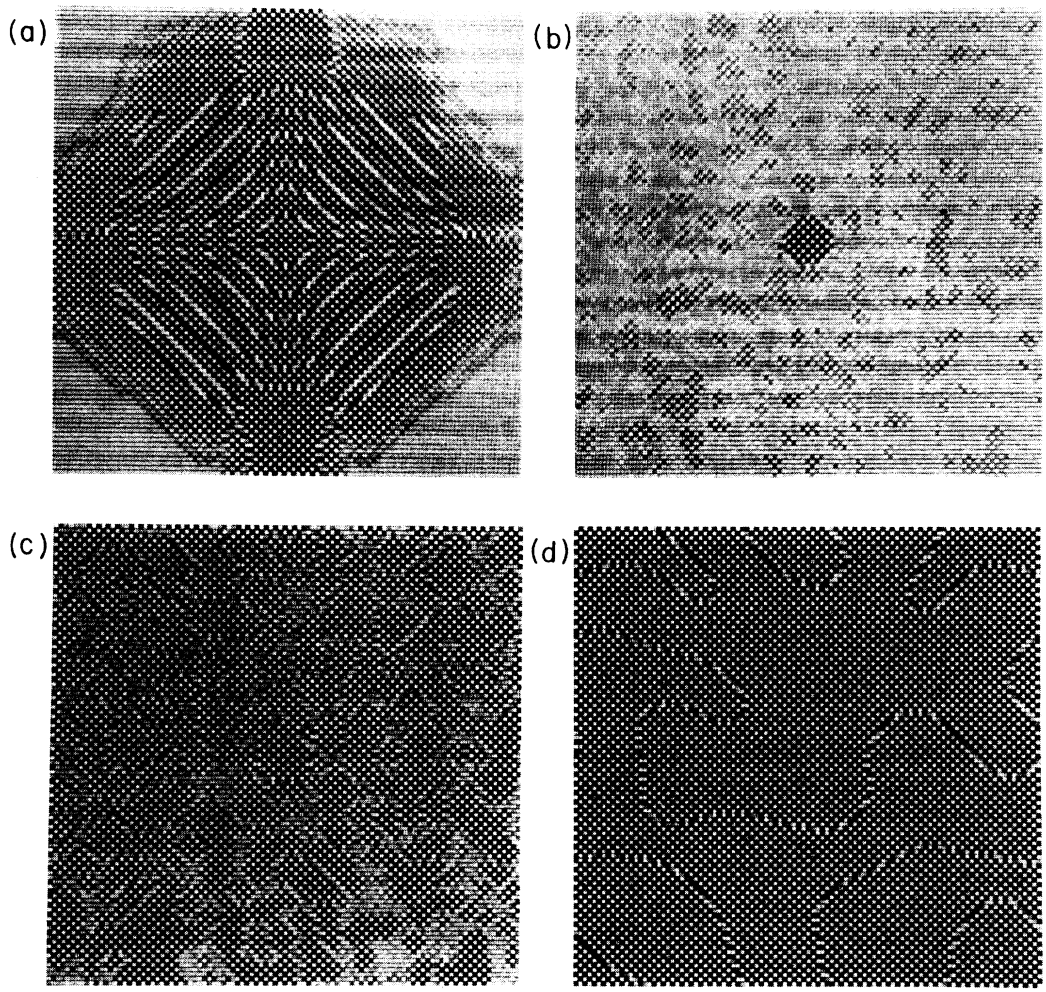

FIG. 10. Evolution from an initial seed for the two-dimensional five-neighborhood model for ($\lambda=3.3$, $\gamma=-0.1$): (a) fragmentation due to the roundoff error at $t=400$, (b)–(d) under external noise $\beta=10^{-5}$, (b) $t=80$, (c) $t=1000$, and (d) $t=2000$.

Upon crossing the -1 boundary of the stability region shown in Fig. 1, a subharmonic bifurcation leading to a strictly alternating state occurs. The new fixed points remain on the third-iterate map and the previous description still applies. However, as γ is tuned the system may undergo a Hopf bifurcation, which converts the alternating fixed points to invariant circles.[5] As γ is increased further the sizes of the circles increase until a crisis between them and the preimage of the unstable point occurs. For larger values of γ, every perturbation of the in-phase state yields spatially and temporally disordered solutions.

A different analysis can be carried out for random-phase initial conditions. As already pointed out, asymptotic solutions with no spatial correlations are most probable. For such solutions, the behavior of a map at a site mimics that of an isolated map with an added noise source; the remainder of the array generates the noise. We have tested this observation by comparing the dynamics of an oscillator in the ring with that of a single noisy quadratic map. Figure 9 shows the good agreement between the invariant densities of the coupled system and the noisy map for $\lambda=3.83$. For the noisy map we used a Gaussian noise source which was roughly scaled (by changing its width and variance) to the distribution of coupling strengths in Eq. (2.1) (deterministic dynamics). Moreover, for λ values corresponding to chaotic motion for the logistic map, this implies fast decay of the temporal correlation function, i.e., fast propagation and amplification of perturbations along the chain. All of these ideas may be generalized to the two-dimensional array and the different types of coupling terms introduced in Sec. II.

V. EXTERNAL NOISE

There is evidence that the evolution of the spatial structure in some parameter regions is quite sensitive to small-amplitude external noise. Consider the evolution from a

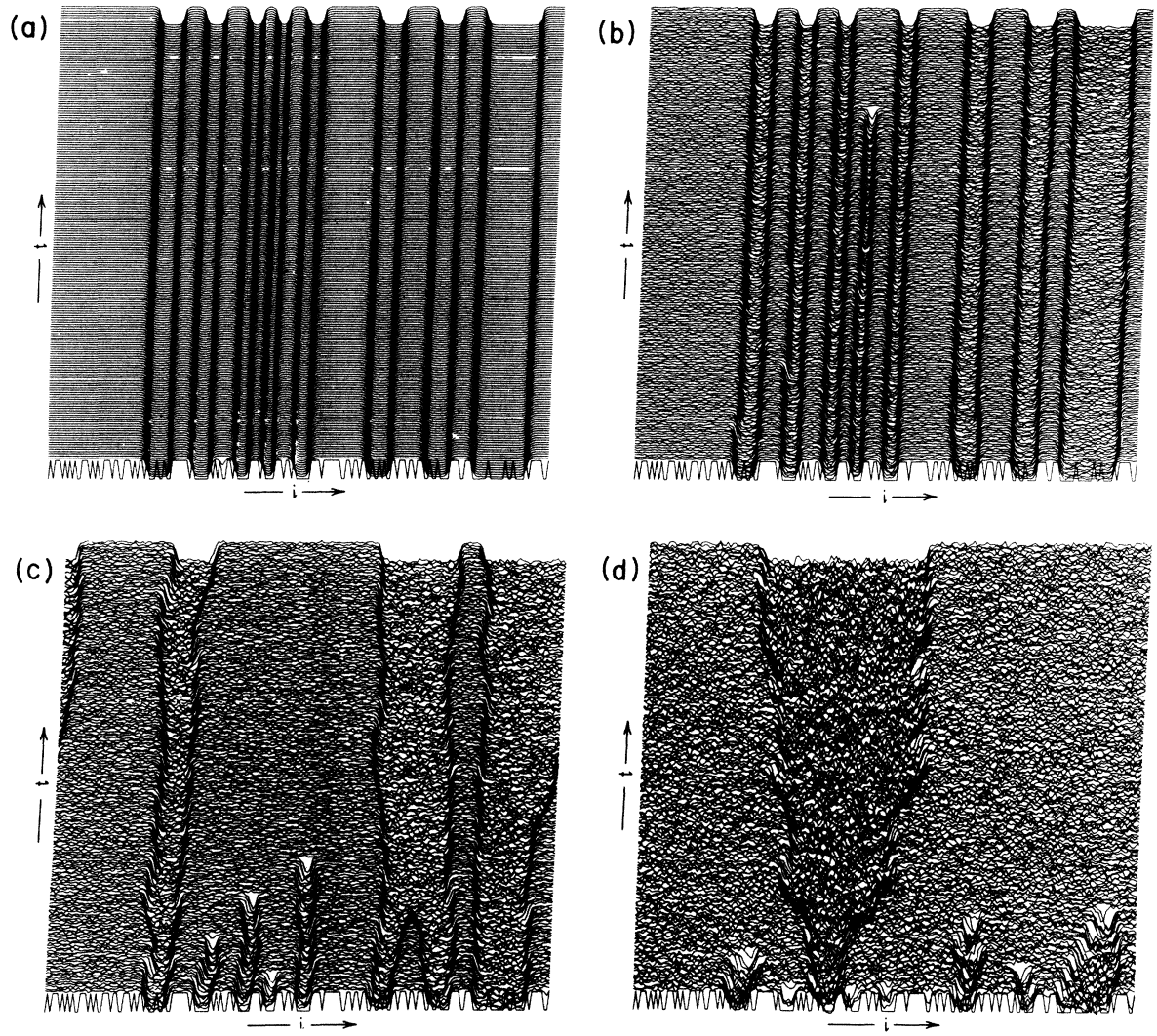

FIG. 11. Temporal evolution of a one-dimensional ring of 200 oscillators for ($\lambda=3.2$, $\gamma=-0.11$) with added external noise (a) $\beta=0$, (b) $\beta=0.01$, (c) $\beta=0.02$, and (d) $\beta=0.04$.

single seed in the region far outside the homogeneous period-2 boundary where there is a long-wavelength instability in addition to one with wavelength 2. As the pattern evolves it fragments as it grows larger [Fig. 10(a)]. This can be attributed to round-off error in the numerical computation.

We can simulate the effects of external noise by the stochastic difference equations

$$x(\mathbf{i},t+1)=f(x(\mathbf{i},t);\lambda)+c(\mathbf{x}(t);\gamma)+\eta(\mathbf{i},t), \quad (5.1)$$

where $\eta(\mathbf{i},t)$ is a random variable taken from a uniform distribution with width β. Figures 10(b)–10(d) show the evolution under the same conditions as above but now using Eq. (5.1) with $\beta=10^{-5}$. Since the homogeneous state is unstable for these parameter values the noise is amplified and after about 80 time steps the inhomogeneties produced by the noise are clearly visible in the figure. Before the original seed has had a chance to evolve it is overwhelmed by the growing patterns from other sites. The system evolves to a checkerboard state with dislocation boundaries, which is quite stable to the small amount of noise present in this simulation.

Dramatic effects on the spatial nature of the final state in presence of noise are also found in the homogeneous parameter regions. Figure 11 shows the temporal evolution of a string of 200 oscillators starting from a random-phase initial condition for $\lambda=3.82$, $\gamma=-0.11$ and four different values of β. As the noise amplitude is increased, kinks and antikinks move along the chain and annihilate upon collision. Thus, noise has the effect of "annealing" defects in the structure and a more homogeneous final state is produced [Fig. 11(d)]. These results should be compared with those near the Hopf bifurcation, which were discussed in Sec. III.

These few results imply that external noise may play an important role in spatial pattern evolution. Stochastic models of spatial structures observed in physical systems may be essential in some circumstances.

VI. DISCUSSION

The results presented in this paper suggest that coupled-map models provide a useful framework for describing a variety of spatio-temporal structures in far-from-equilibrium systems. The behavior of the system can be studied as a function of control parameters characterizing the oscillators and their coupling. Furthermore, they lend themselves to bifurcation analyses as shown, for example, in Sec. II where generalized expressions for boundary curves for homogeneous states were obtained for any number of coupled oscillators, for a variety of interaction models, and for different spatial dimensions. Moreover, bifurcation theory can be used to construct mechanisms for a number of dynamical phenomena involving spatial structures. The mechanisms for the destruction of the dislocation boundaries and the evolution of chaotic patterns near intermittency provide examples of such analyses.

While the models discussed in this paper were not intended to model a particular system, the phenomena observed bear many similarities to the spatio-temporal structures in physical systems. The results presented here could provide guides to the nature of the origin and dynamics of particular spatial structures which have not yet been observed.

Furthermore, coupled-map models are characterized by deterministic rules of interaction among sites and are thus similar to cellular automata. Indeed, generalizations of the excitable-medium automaton are akin to the models discussed here. The exploration of these and related models with a direct physical basis is a worthwhile endeavor.

ACKNOWLEDGMENTS

We wish to thank E. Celarier, S. Fraser, S. Ruffo, and S. G. Whittington for useful discussions and M. Peterson for computer assistance. This research was supported in part by a grant from the Natural Sciences and Engineering Research Council of Canada.

[1] *Oscillations and Traveling Waves in Chemical Systems*, edited by R. J. Field and M. Burger (Wiley, New York, 1985); G. Nicolis and I. Prigogine, *Self-Organization in Nonequilibrium Systems* (Wiley, New York, 1977).

[2] S. Wolfram, Rev. Mod. Phys. **55**, 601 (1983); *Cellular Automata*, edited by D. Farmer, T. Toffoli, and S. Wolfram (North-Holland, New York, 1984); N. Packard and S. Wolfram, J. Stat. Phys. **38**, 901 (1985).

[3] J. M. Greenberg, B. D. Hassard, and S. P. Hastings, Bull. Am. Math. Soc., **84**, 1296 (1978); J. M. Greenberg and S. P. Hastings, SIAM J. Appl. Math. **34**, 515 (1978); W. Freedman and B. Madore, Science **222**, 615 (1983).

[4] A. T. Winfree, E. M. Winfree, and H. Seifert, Physica **17D**, 109 (1985).

[5] I. Waller and R. Kapral, Phys. Rev. A **30**, 2047 (1984); R. Kapral, *ibid.* **31**, 3868 (1985).

[6] K. Kaneko, Prog. Theor. Phys. **69**, 1427 (1983); **72**, 480 (1984).

[7] J. D. Keeler and J. D. Farmer (unpublished).

[8] K. Kaneko, Prog. Theor. Phys. **74**, 1033 (1985).

[9] See, for instance, P. Ortoleva, in *Theoretical Chemistry*, edited by H. Eyring and D. Henderson (Academic, New York, 1978), p. 235; A. T. Winfree, *ibid.*, p. 1; N. Koppel and L. Howard, Stud. Appl. Math. **52**, 291 (1973).

[10] Y. Oono and M. Kohmoto, Phys. Rev. Lett. **55**, 2327 (1985).

[11] Such slow evolution of dislocation structures in nonequilibrium systems has been observed in experiments on convective instabilities. See S. Ciliberto and J. P. Gollub, Phys. Rev. Lett. **52**, 922 (1984); M. S. Heutmaker, P. N. Fraenkel, and J. P. Gollub, *ibid.* **54**, 1369 (1985); M. Lowe and J. P. Gollub, Phys. Rev. A **31**, 3893 (1985).

[12] R. Kapral, E. Celarier, and S. Fraser, in *Fluctuations and Sensitivity in Nonequilibrium Systems*, edited by W. Horsthemke and D. K. Kondepudi (Springer-Verlag, New York, 1984), p. 179.

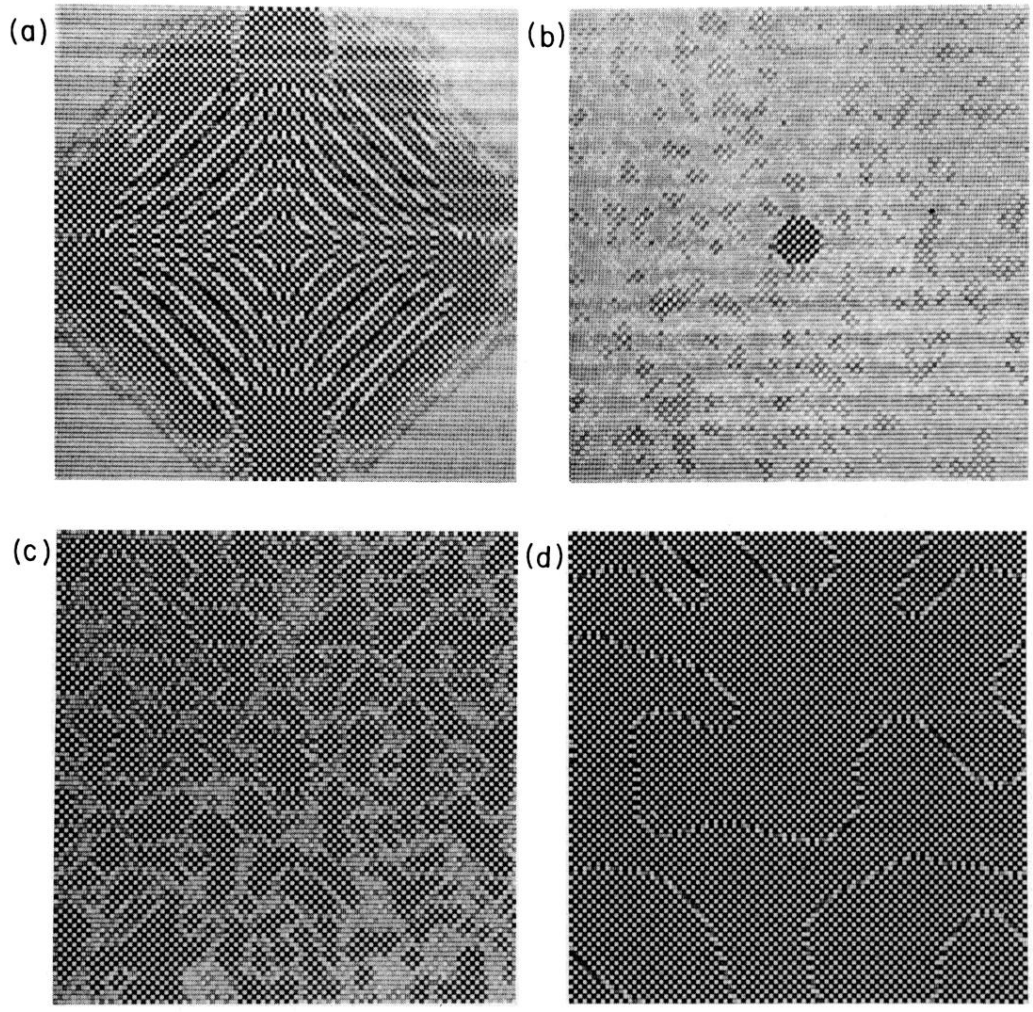

FIG. 10. Evolution from an initial seed for the two-dimensional five-neighborhood model for ($\lambda=3.3$, $\gamma=-0.1$): (a) fragmentation due to the roundoff error at $t=400$, (b)–(d) under external noise $\beta=10^{-5}$, (b) $t=80$, (c) $t=1000$, and (d) $t=2000$.

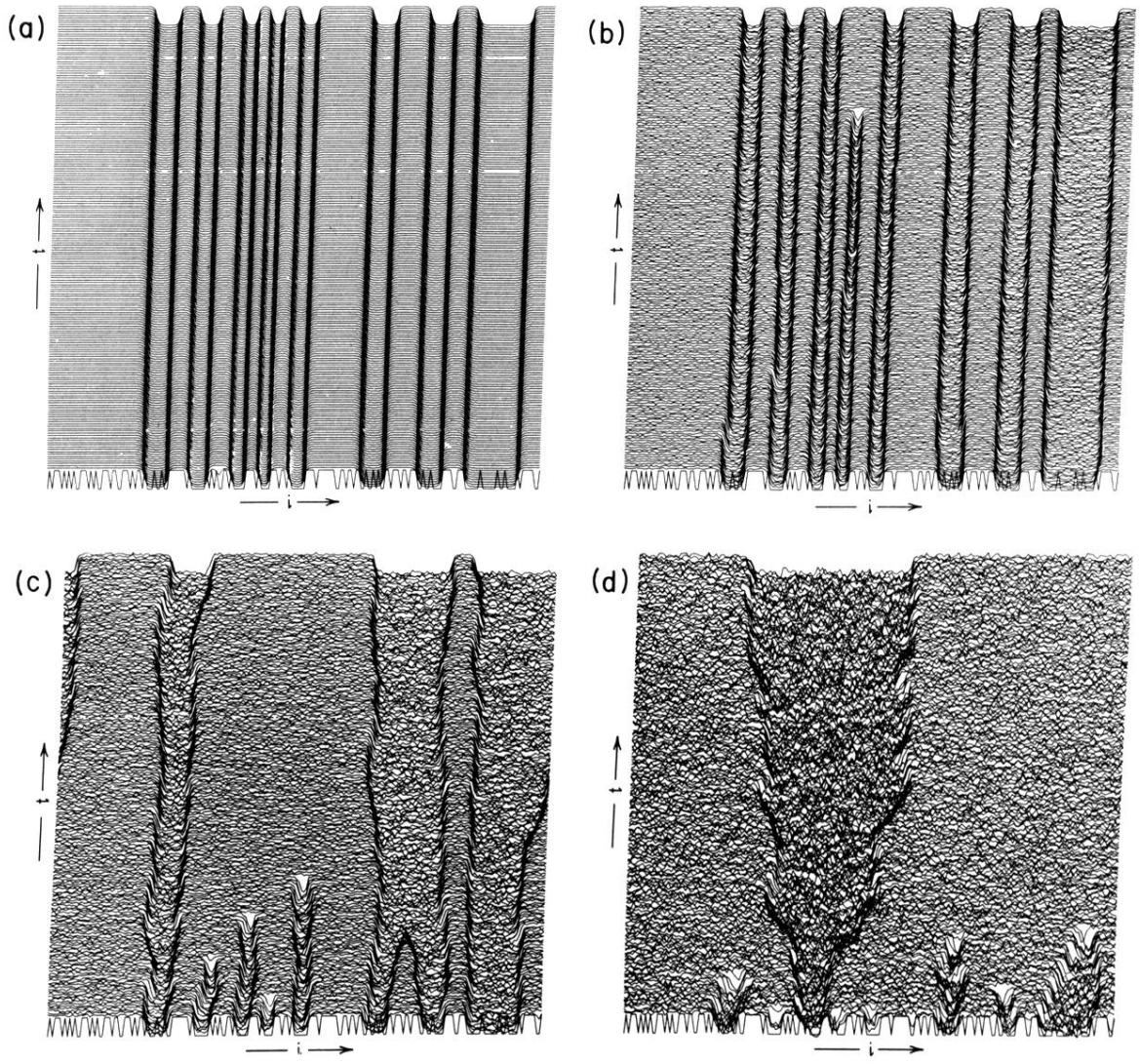

FIG. 11. Temporal evolution of a one-dimensional ring of 200 oscillators for ($\lambda=3.2$, $\gamma=-0.11$) with added external noise (a) $\beta=0$, (b) $\beta=0.01$, (c) $\beta=0.02$, and (d) $\beta=0.04$.

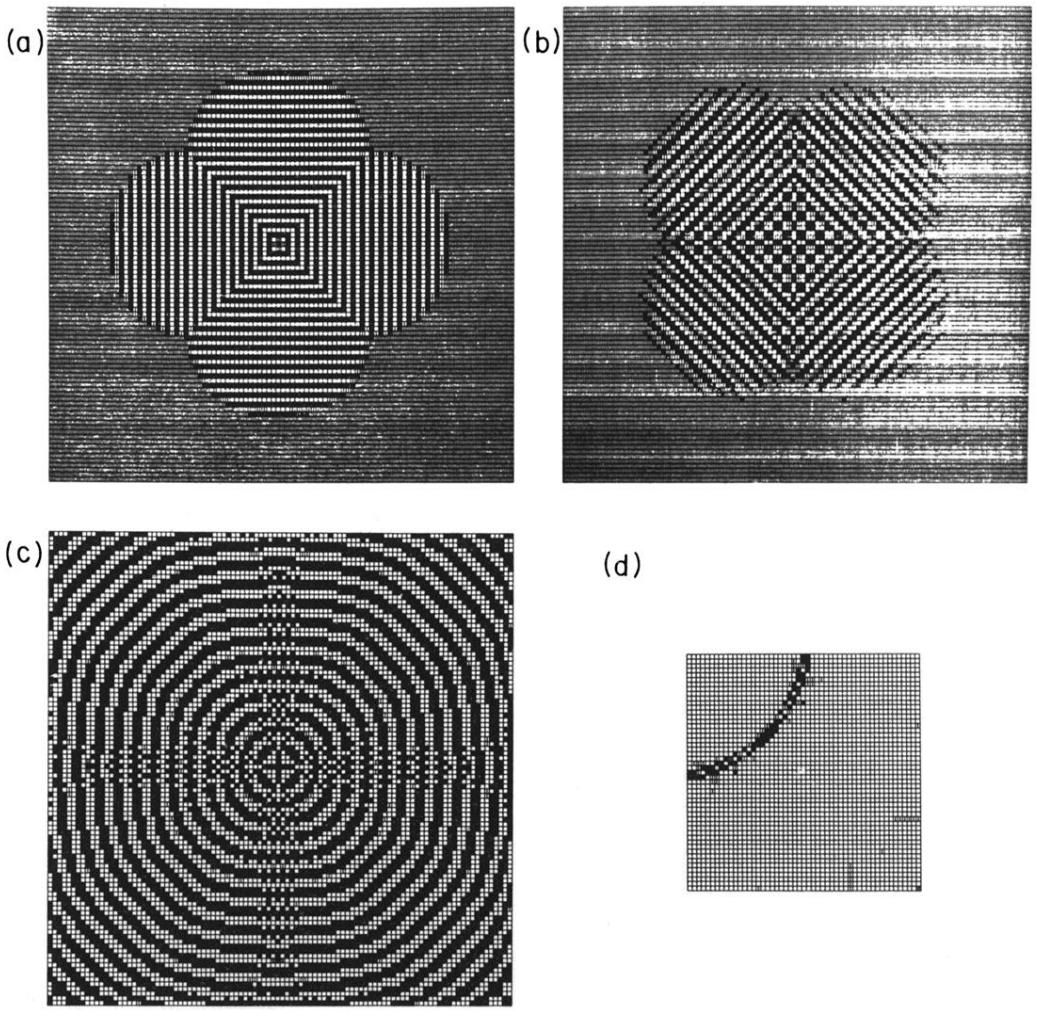

FIG. 2. Evolution from an initial seed for a 100×100 two-dimensional array of maps: (a) nine-neighborhood model with ($\lambda = 3.30$, $8\gamma = -0.4$) at $t = 400$, (b) thirteen-neighborhood model with ($\gamma = 3.30$, $12\gamma = -0.4$) at $t = 400$, (c) thirteen-neighborhood model with ($\lambda = 3.30$, $12\gamma = -1.0$) at $t = 400$. The shading of a square indicates the magnitude of x at that site. (d) Spatial Fourier transform of the pattern given in (c).

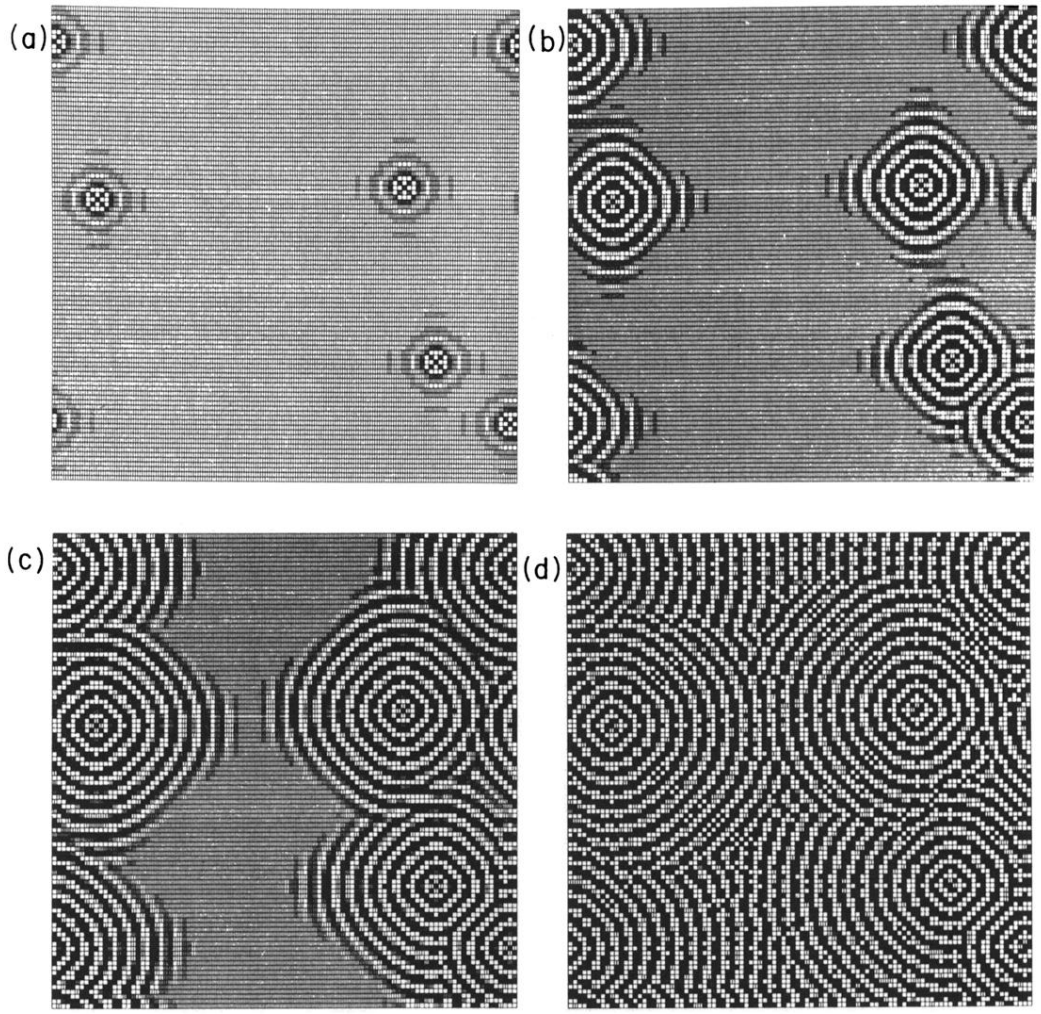

FIG. 3. Evolution from a random spatial distribution of five initial seeds for the two-dimensional nine-neighborhood model with ($\lambda=3.30$, $\gamma=-0.125$) at (a) $t=40$, (b) $t=80$, (c) $t=120$, and (d) $t=1600$.

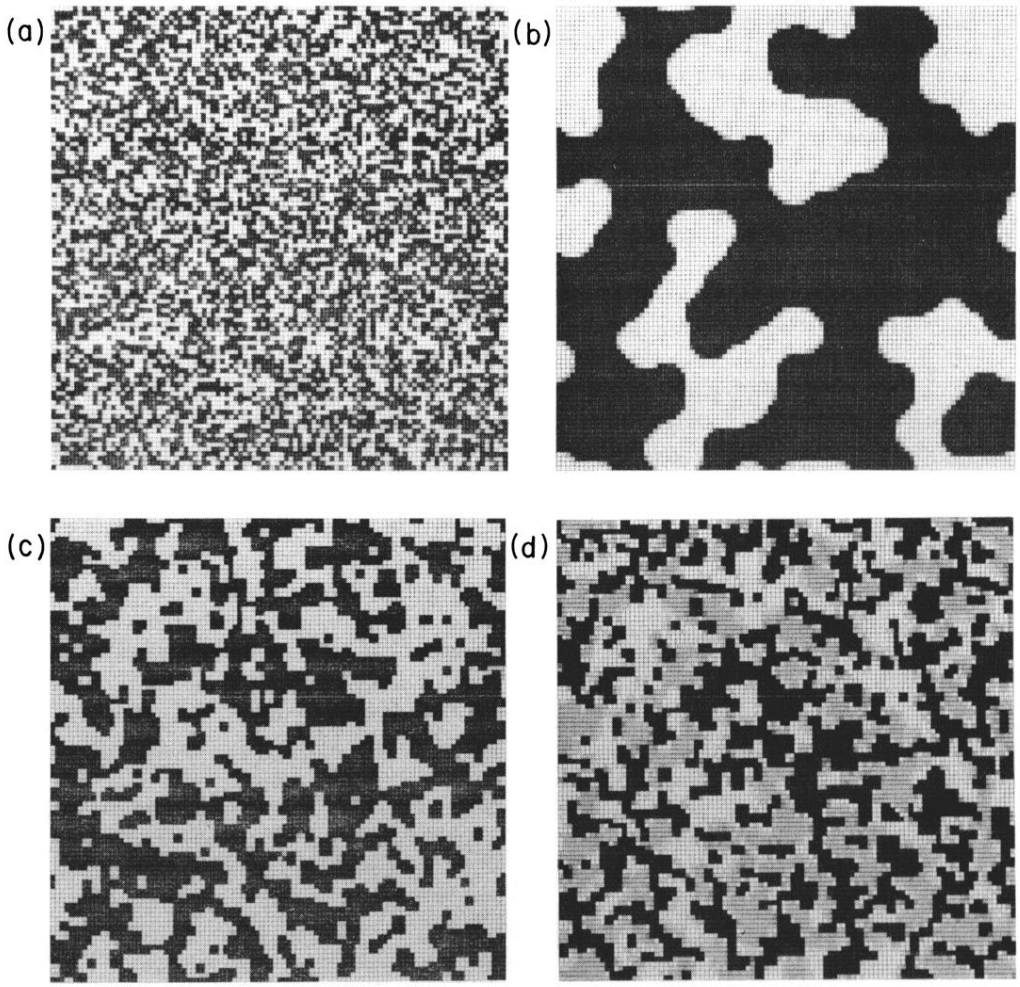

FIG. 4. Time evolution from an initial random-phase distribution for the two-dimensional five-neighborhood model with (a) ($\lambda=3.2$, $\gamma=-0.05$), period-2 region, at $t=2$, (b) ($\lambda=3.2$, $\gamma=-0.05$), period-2 region at $t=4000$, (c) ($\lambda=3.2$, $\gamma=-0.025$), period-2 region, at $t=4000$, and (d) ($\lambda=3.48$, $\gamma=-0.035$), period-4 region, at $t=4000$.

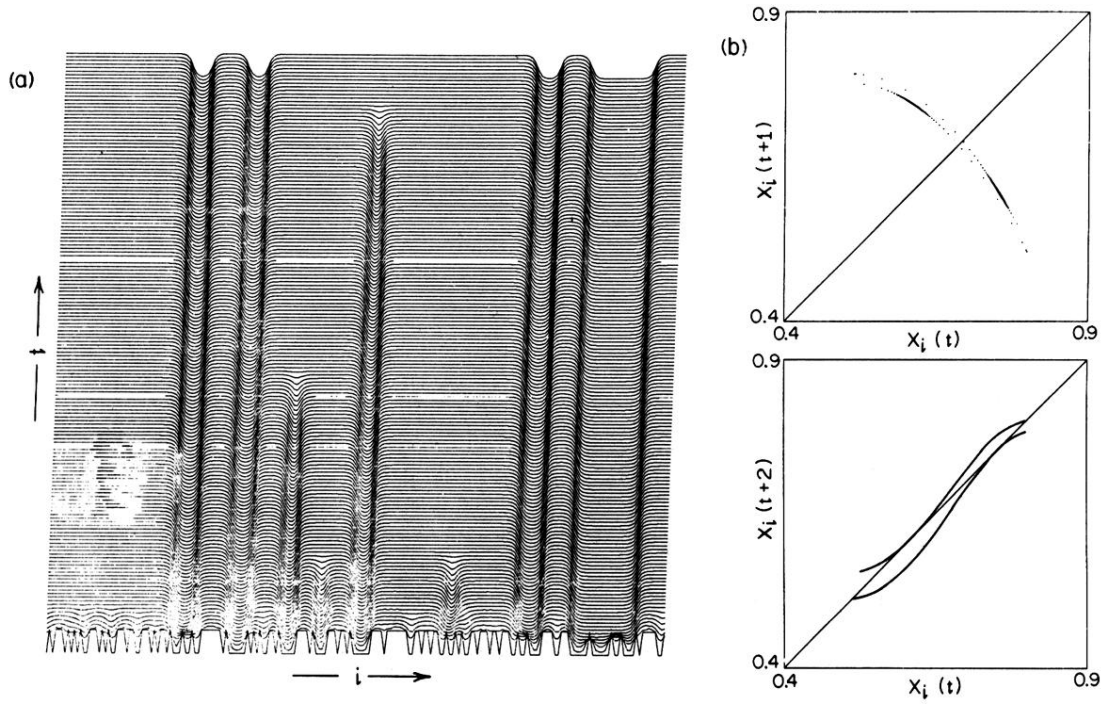

FIG. 5. (a) Time evolution of an initial random distribution of the two period-2 phases for 200 coupled maps in a one-dimensional chain. The ordinate is time and the abscissa is the site index. The results are plotted every two time steps up to $t=320$ with ($\lambda=3.2$, $\gamma=-0.25$). (b) First and second next-amplitude maps for the single out-of-phase oscillator in an otherwise homogeneous chain with ($\lambda=3.2$, $\gamma=-0.02775$). Solid lines have been drawn through the points in order to make the "tangent character" of the map evident.

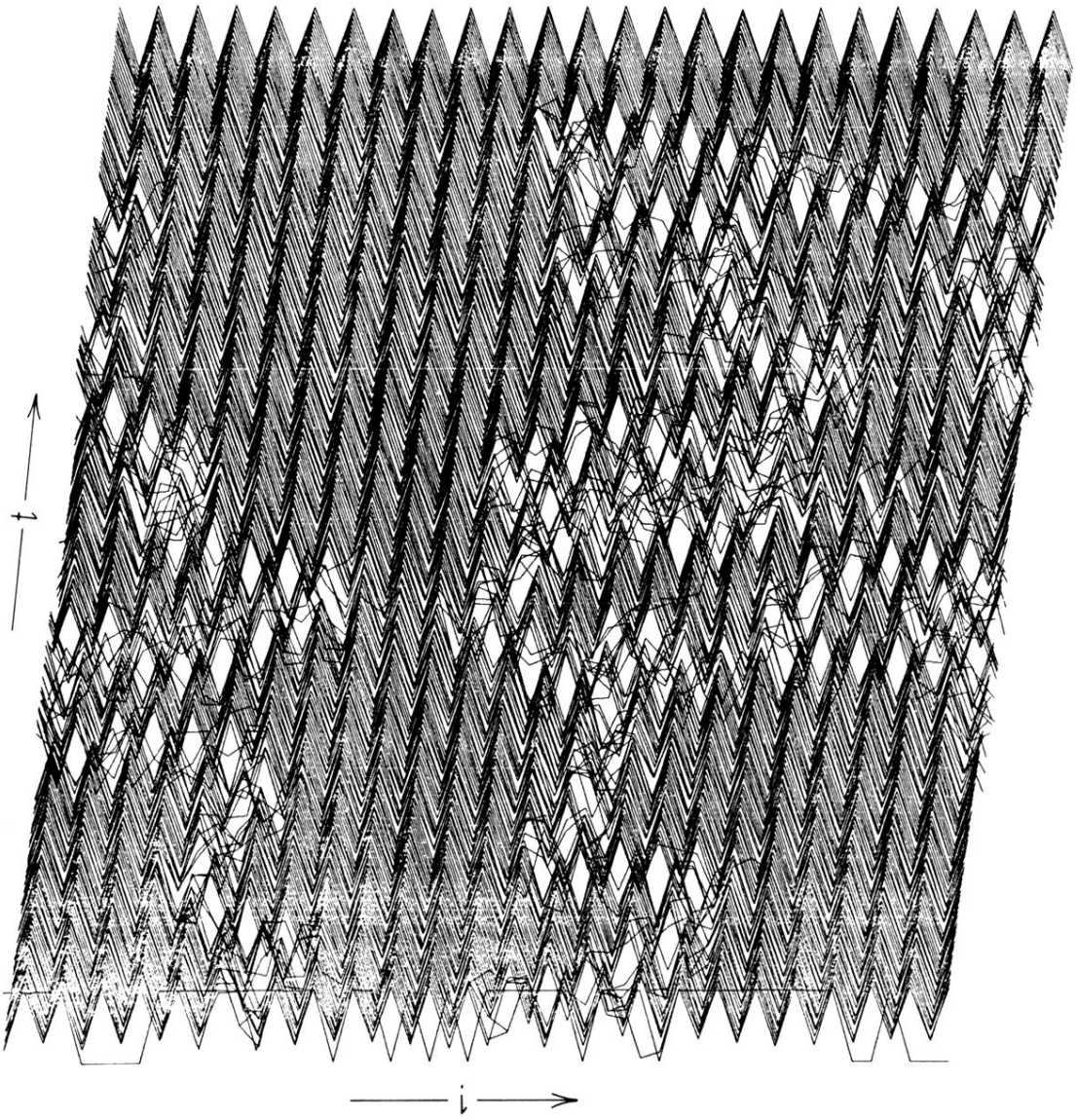

FIG. 7. Dislocation dynamics in a strictly alternating pattern. Starting from a random-phase initial condition with ($\lambda = 3.748$, $\gamma = -0.07$), a purely alternating state is reached after approximately 13 000 time steps.